Water Research 186 (2020) 116324

Contents lists available at ScienceDirect

Water Research

journal homepage: www.elsevier.com/locate/watres

Impact of CeO_2 nanoparticles on the aggregation kinetics and stability of polystyrene nanoplastics: Importance of surface functionalization and solution chemistry

Xing Li[a], Erkai He[b], Bing Xia[c], Cornelis A.M. Van Gestel[d], Willie J.G.M. Peijnenburg[e,f], Xinde Cao[a], Hao Qiu[a,*]

[a] School of Environmental Science and Engineering, Shanghai Jiao Tong University, Shanghai, 200240, China
[b] School of Geographic Sciences, East China Normal University, Shanghai, 200241, China
[c] Anhui Academy of Environmental Science Research, Hefei 230022, China
[d] Department of Ecological Science, Faculty of Science, Vrije Universiteit, Amsterdam, 1081HV, The Netherlands
[e] Institute of Environmental Sciences, Leiden University, Leiden 2333CC, The Netherlands
[f] National Institute of Public Health and the Environment, Center for the Safety of Substances and Products, Bilthoven 3720BA, The Netherlands

ARTICLE INFO

Article history:
Received 8 July 2020
Revised 18 August 2020
Accepted 19 August 2020
Available online 20 August 2020

Keywords:
Engineered nanoparticles
Surface functional groups
Hydrochemical condition
Stability

ABSTRACT

The increasing application of plastics is accompanied by increasing concern over the stability and potential risk of nanoplastics. Heteroaggregation with metal-based nanoparticles (e.g., CeO_2-NPs) is critical to the environmental mobility of nanoplastics, as they are likely to be jointly emitted to the aquatic environment. Here, time-resolved dynamic light scattering was employed to evaluate the influence of CeO_2-NPs on the aggregation kinetics of differentially surface functionalized polystyrene nanoplastics (PS-NPs) in various water types. Natural organic matters and ionic strength were dominating factors influencing the heteroaggregation of PS-NPs and CeO_2-NPs in surface waters. The critical coagulation concentrations of PS-NPs were dependent on their surface coatings, which decreased in the presence of CeO_2-NPs due to electrostatic attraction and/or specific adsorption. Incubation of PS-NPs and CeO_2-NPs under different pH confirmed the importance of electrostatic force in the aggregation of PS NPs. A relatively low humic acid (HA) concentration promoted the heteroaggregation of NH_2-coated PS-NPs and CeO_2-NPs because the introduction of a HA surface coating decreased the electrostatic hindrance. At high HA concentrations, the aggregation was inhibited by steric repulsion. The combined effects of high efficiency of double layer compression, bridging and complexation contributed to the high capacity of Ca^{2+} in destabilizing the particles. These findings demonstrate that the environmental behavior of nanoplastics is influenced by the presence of other non-plastic particles and improve our understanding of the interactions between PS-NPs and CeO_2-NPs in complex and realistic aqueous environments.

1. Introduction

We are living in a plastic age. Plastics are commonly present in our daily life, ranging from packaging to construction materials, electronics, aerospace, and automobile (Hernandez et al., 2017; Zhang et al., 2017). The widespread use of commercial products containing plastics and the poor disposal of plastic waste have caused a large amount of plastic debris accumulating in the environment (Napper and Thompson, 2016; Halle et al., 2016). Researchers have investigated the distribution of plastics, and found that they are widely distributed in oceans, rivers, sediments, and soils (Cózaret al., 2014; Blettler et al., 2019; Lorenz et al., 2019; He et al., 2020). It is worth noting that the larger plastic fragments present in the ambient environment can break down into small-sized particles, namely microplastics ($< 5\ \mu m$) and nanoplastics ($<$ 100 nm) via abiotic (UV radiation, mechanical abrasion, and weathering) and biotic (biodegradation) processes (Halle et al., 2016; Enfrin et al., 2019). Especially, nano-sized plastics, possessing small size and high specific area to volume ratio, are attracting increasing attention because they are more easily ingested by organisms, and may accumulate in food chains, thus finally posing potential risks to ecosystems and humans (Wright et al., 2013; Cole et al., 2015; Dawson et al., 2018).

The number of investigations on the environmental behavior, fate and toxicity of nanoplastics has increased exponentially, as

* Corresponding author.
E-mail address: haoqiu@sjtu.edu.cn (H. Qiu).

https://doi.org/10.1016/j.watres.2020.116324
0043-1354/

nanoplastics have become a significant environmental concern. Many researchers focused on nanoplastics aggregation due to its importance in water and wastewater treatment processes, and subsequently transport, sedimentation, bioavailability and toxicity (Dong et al., 2019; Wu et al., 2019; Enfrin et al., 2020a, 2020b). Various factors can influence the colloidal stability and aggregation kinetics of nanoplastics in aqueous environments. For example, Cai et al. (2018) reported that significant aggregation of nanoplastics occurred in the presence of Fe^{3+} as compared to Na^{+} and Ca^{2+}. Singh et al. (2019) showed that higher temperature affected the kinetic energy of nanoplastics, making them unstable in aquatic media. Recently, Yu et al. (2019) found that natural organic matter reduced the aggregation of nanoplastics in NaCl solution by steric hindrance, while the Ca^{2+} bridging effect and carboxyl complexion accelerated nanoplastic aggregation. The above-mentioned studies revealed that the prevailing physical and chemical conditions of the aquatic environment basically drive the homoaggregation behavior of nanoplastics. Additionally, with the increasing application of engineered nanoparticles (ENPs), it is highly likely that nanoplastics and ENPs could interact with each other, resulting in the formation of heteroaggregates (Dong et al., 2019). The studies of Cai et al. (2019) and Singh et al. (2019) confirmed that the presence of other nanoparticles was responsible for the heteroaggregation and transport of nanoplastics. Oriekhova and Stoll, (2018) reported that the colloidal stability and particle sizes of nanoplastics were closely related with the mass ratio of nanoplastics/Fe_2O_3 NPs under experimental conditions. So far, no specific studies have been performed to depict the heteroaggregation of nanoplastics and ENPs under realistic environmental conditions. The dominating environmental factors influencing the interaction between nanoplastics and ENPs thus remain unclear.

It was indicated that the surface properties of ENPs controlled the interfacial interaction and heteroaggregation of ENPs (e.g. Ag NPs, graphene oxide), as well as the subsequent toxicity (Lodeiro et al., 2018; Zhao et al., 2018). Plastics debris, it may undergo chemical reaction and form new functional groups after discharged into the environments, which will further influence their surface properties and colloidal stability (Gewert et al., 2015; Yu et al., 2019). However, the existing studies regarding interaction between nanoplastics and ENPs mainly concentrated on single nanoplastics, and neglected the importance of surface properties of nanoplastics, which thus cannot allow full understanding of their environmental behavior (Cai et al., 2019; Dong et al., 2019; Yu et al., 2019). Furthermore, the interaction force may vary dependent on the surface properties of the ENPs. For instance, Wang et al. (2015) reported that humic acid modified the surface of Ag NPs, and inhibited their heteroaggregation with kaolin due to steric repulsion. Song et al. (2019) compared colloidal stability of nano-particulate biochar derived from different feedstock sources, showing that biochar with more O-containing functional surface groups tends to complex or coprecipitate with other pollutants. To understand the heteroaggrergation behavior and exact mechanism of emerging nanoplastics in a more realistic environment with other coexisting nanoparticles, further studies are needed which take the specificity of surface functional groups into account.

In the present study, the heteroaggregation of polystyrene nanoplastics (PS NPs) with artificially produced nanoparticle was investigated in natural waters and in experimental solutions. Cerium dioxide NPs (CeO_2 NPs), a typical engineered nanoparticle widely applied in industry and commercial products (Fall et al., 2007; Piccinno et al., 2012), was selected as a model manufactured nanoparticle. We hypothesize that there were significant differences in heteroaggregation kinetics due to the surface functionalization of PS NPs and the complex physicochemical properties of surface waters. To verify this hypothesis, time-resolved dynamic light scattering was employed to characterize the heteroaggregation profiles of PS NPs with different surface properties (none, carboxyl, amine, epoxy and sulfonic) and CeO_2 NPs in a diverse array of natural surface waters, including sea water, river water, lake water, and ground water. The underlying interaction forces between PS NPs and CeO_2 NPs were revealed by the application of Fourier Transform Infrared spectrometer and X-ray photoelectron spectroscopy.

2. Materials and methods

2.1. Chemicals

Aqueous suspensions of PS-Bare, PS-COOH, PS-NH_2, PS-C_2H_2O, and PS-SO_3H with a concentration of 10% w/v, were obtained from Shanghai Huge Biotechnology Co., Ltd. (Shanghai, China). The primary particle size of PS-SO_3H was 80 nm, whereas the nominal size of the other modified PS particles was 50 nm, according to the manufacturer. CeO_2 NPs power with nominal particle diameter $<$ 25 nm was purchased from Sigma Aldrich (USA). The morphological properties, size distribution, and point of zero charge (PZC) of all nanoparticles were determined with a transmission electron microscopy (TEM) (Tecani G^2 Spirit TWIN, FEI, Netherlands) and Malvern Zetasizer Nano ZS90 (Malvern, Worcestershire, UK), respectively. The details were described in our previous study (Li et al., 2020). Humic acid (HA) was used as the representative natural organic matter (Sigma Aldrich, USA). HA stock suspensions with a concentration of 10.8 mg C/L were prepared following the method described earlier (Li et al., 2020). The stock suspensions were stored at 4°C before use.

2.2. Natural water samples

Eight natural waters, including sea water (SW), lake water (LW), river water (RW), and ground water (GW), were sampled and filtered through a 0.45 μm mixed cellulose ester membrane under vacuum. The ionic composition and total organic carbon (TOC) content was analyzed by ionic chromatographic analyzer (ICS-5000, Thermo Fisher) and TOC analyzer (TOC-V, Shimadzu, Japan). The samples were preserved at 4°C before use. Details on sampling site and physicochemical properties of the water samples are given in the Supplementary Material (Table S1 and S2).

2.2. Aggregation experiments

The suspensions were prepared just before use and sonicated for 30 min at 120 W to obtain a homogeneous system before the batch experiments. The pH of the suspensions was adjusted to 5.0 $\pm$ 0.1 with either 0.1 M HCl or 0.1 M NaOH solution, unless specifically pointed out. The final concentration of PS NPs and CeO_2 NPs was 10 mg/L, and 20 mg/L for achieving convenient aggregation rates, respectively.

The aggregation experiments were performed using time-resolved dynamic light scattering (TR-DLS, Malvern Zetasizer Nano ZS90, Malvern, Worcestershire, UK) with 173° scattering angle under different water chemistry. The hydrodynamic diameter (D_h) was recorded every 30 s continuously for 30 min, with no delay between measurements. The heteroaggregation kinetics of PS NPs with CeO_2 NPs in natural waters or experimental solutions were initiated by adding an aliquot of the PS NPs and CeO_2 NPs suspension into SW, LW, RW, GW, and electrolyte solution (NaCl and $CaCl_2$) with or without HA. The assessment of the homoaggregation kinetics of PS NPs and CeO_2 NPs induced by NaCl and $CaCl_2$ followed a similar procedure.

The aggregation rate constant (k) was obtained from the slope of the aggregation profile. The slope can be calculated by linear

regression of the D_h exceeding 1.5 times its initial value (D_0), which is proportional to ($dD_h(t)/dt$) Chen and Elimelech, 2006:

$$k \propto \frac{1}{N_0}\left(\frac{dD_h(t)}{d(t)}\right) t \to 0 \quad (1)$$

Here N_0 is the initial particle concentration (mg/L), and $D_h(t)$ is the average hydrodynamic diameter (nm) at time t.

The attachment efficiency (α) was used to reflect the aggregation kinetics. The α is calculated by normalizing the ratio of the aggregation rate in the reaction-limited regime (k) to that in the diffusion-limited regime (k_{fast}) in a certain solution as follows:

$$\alpha = \frac{k}{k_{fast}} = \frac{\frac{1}{N_0}\left(\frac{dD_h(t)}{d(t)}\right) t \to 0}{\frac{1}{(N_0)_{fast}}\left(\frac{dD_h(t)}{d(t)}\right) t \to 0, fast} \quad (2)$$

2.3. Cryonic transmission electron microscopy

The conventional transmission electron microscopy (TEM) technique with sample drying cannot reproduce the correct aggregates structure and size, and will inevitably result in agglomeration. Hence, the cryonic TEM (cryo-TEM, Talos F200C G^2, FEI, USA), which is optimal for observing the *in-situ* morphology of colloids in solutions, was employed in the present study to visualized the morphology of heteroaggregates of PS NPs with CeO_2 NPs in SW-X and LW-S. In detail: 3 μL of the selected samples was deposited on a carbon-coated copper grid that had been ionized in a Femto plasma cleaner (Diener Electronic, Germany) for 60 s. The grid was then blotted by filter paper, placed on a vitrification robot (Vitrobot, FEI Vitrobot Mark IV), and ultrafast-frozen in liquid ethane to achieve a thin layer of vitreous ice. The vitrified specimens were kept in liquid nitrogen until they were inserted into a cryo-TEM-holder Gatan 626 (Gatan Inc., USA) for analysis.

2.4. Spectral analysis

To obtain heteroaggregates of PS NPs with CeO_2 NPs, heteroaggregation suspensions were prepared by mixing CeO_2 NPs and PS NPs in NaCl, $CaCl_2$, or HA solution at pH = 5. After heteroaggregation for 30 min, the mixture was freeze-dried for spectral analysis. Fourier Transform Infrared spectrometer (FTIR, Nicolet, Madison, WI, USA) was used to investigate the changes of functional groups and surface structures before and after heteroaggregation at the spectral range of 4000 ~ 400 cm^{-1}. The surface elemental composition was identified by X-ray photoelectron spectroscopy (XPS, AXIS UltraDLD, Shimadzu, Japan), with a magnesium Kα X-ray source (1253.5 eV). Survey spectra were recorded from 1200 ~ 0 eV for each sample in a vacuum of 10^{-8} Pa. All peaks were calibrated using C1s peak at 284.8 eV. The data was processed using the CacaXPS software.

2.5. Derjaguin-landau-verwey-overbeek calculations

To revel the underlying interaction mechanisms between PS NPs and CeO_2 NPs, the net energy barrier between PS NPs and CeO_2 NPs under different electrolytes and different IS was calculated based on the Derjaguin-Landau-Verwey-Overbeek (DLVO) theory. Detailed calculations are presented in the Supplementary information (Text S1).

3. Results and discussion

3.1. Characterization

The particle size, morphology, and hydrodynamic diameter of PS NPs and CeO_2 NPs were determined using TEM and DLS measurements (Fig. S1 and Table S3). As evident from the results of TEM, the five PS NPs displayed spherical morphology with an average diameter of ~50 nm for PS-Bare, PS-COOH, and PS-C_2H_2O, and ~80 nm for PS-NH_2 and PS-SO_3H. The hydrodynamic diameter of PS-Bare, PS-COOH, and PS-C_2H_2O was basically equal to its diameter, meaning these PS NPs were fairly stable. In contrast, the hydrodynamic diameter of PS-NH_2 and PS-SO_3H was larger than the value of the diameter obtained by TEM. This size difference can be attributed to the polymer layer and the hydration shell adsorbed on PS NPs surfaces (Yu et al., 2019; Wang et al., 2020). The CeO_2 NPs were either cubic or pyramidal of shape with a mean diameter of 25 nm. The much larger hydrodynamic diameter of CeO_2 NPs can be ascribed to the formation of homo-aggregates in suspension (Tiwari et al., 2020).

In Fig. S2, the zeta potential of the particles is displayed as a function of pH. The surface charge of PS-Bare, PS-COOH, PS-C_2H_2O, and PS-SO_3H remained negative over a wide range of pH levels, indicating that the point of zero charge (pH_{PZC}) was beyond the pH range investigated. Since pH in the aquatic environment typically ranges from 5.0 to 9.0, these four PS NPs would be stable for a long period in the aqueous environment, posing a serious environmental concern (Li et al., 2018). The zeta potential of PS-NH_2 decreased from 41.2 to - 2.5 mV as the pH increased from 3.0 to 10, with pH_{PZC} = 7.5. In this present study, the homo-, and hetero-aggregation kinetics were assessed at pH 5.0 where the absolute zeta potentials of the NPs exceed a value of 30 mV, which was favorable for assessing their aggregation kinetics.

3.2. Heteroaggregation kinetics of PS NPs with CeO_2 NPs in surface waters

Natural environments are highly heterogeneous systems where CeO_2 NPs and PS NPs are likely to coexist. Here, the heteroaggregation kinetics of PS NPs and CeO_2 NPs in natural aquatic matrices were first explored. For four negatively charged PS NPs, noticeable aggregation was observed in SW-X, while negligible aggregation was found in RW, LW, and GW (Fig. 1). This difference can be explained by the significant difference in the physicochemical properties of the surface water samples (Table S2). As SW-X had the highest ionic strength (IS), particles can form aggregates rapidly due to electrostatic screening. However, the aggregation was inhibited in RW, LW, and GW because of steric hindrance induced by natural organic matter (NOM). In term of chemical compositions, dissolved organic carbon (DOC) content of SW-S and SW-X was similar, but SW-S possessed a lower IS, which thus cannot overcome the steric repulsion arising from the NOM corona on the surface of the particles. This result implies that particles may suspend in sea water with high NOM content. Cryo-TEM samples were obtained on a controlled environment vitrification system, which can *in-situ* visualized the heteroaggregates morphology of PS NPs and CeO_2 NPs in SW-X and LW-H (Fig. 2). In SW-X, the CeO_2 NPs clusters clearly became larger and were bound with PS-Bare aggregates, forming larger and more compact heteroaggregates (Figs. 2a and b). Similarly, CeO_2 NPs clusters attached on the surfaces of PS-Bare in LW-H, but the heteroaggregates were visibly smaller and in a sparse state of aggregation (Figs. 2c and d). These results confirmed the formation of heteroaggregates, which was consistent with the DLS results.

As shown in Figs. 1c and f, the positively charged PS-NH_2 and CeO_2 NPs tended to aggregate in SW-X, SW-S, and LW-S, with average hydrodynamic diameters exceeding 800 nm after heteroaggregation for 30 min. The combined effect of high NOM content and high IS in sea water samples resulted in reversion of the surface potential and destabilization of PS-NH_2 and CeO_2 NPs. Due to the low IS, negligible aggregation was observed in RW-N, RW-Y, LW-H, and GW-H. Compared to the negatively charged PS NPs, NH_2 modified PS NPs showed fast aggregation in GW-S. This can be attributed to the high anion concentrations in GW-S (213 mg/L Cl^-, 423 mg/L SO_4^{2-}), which favored adsorption on the positively

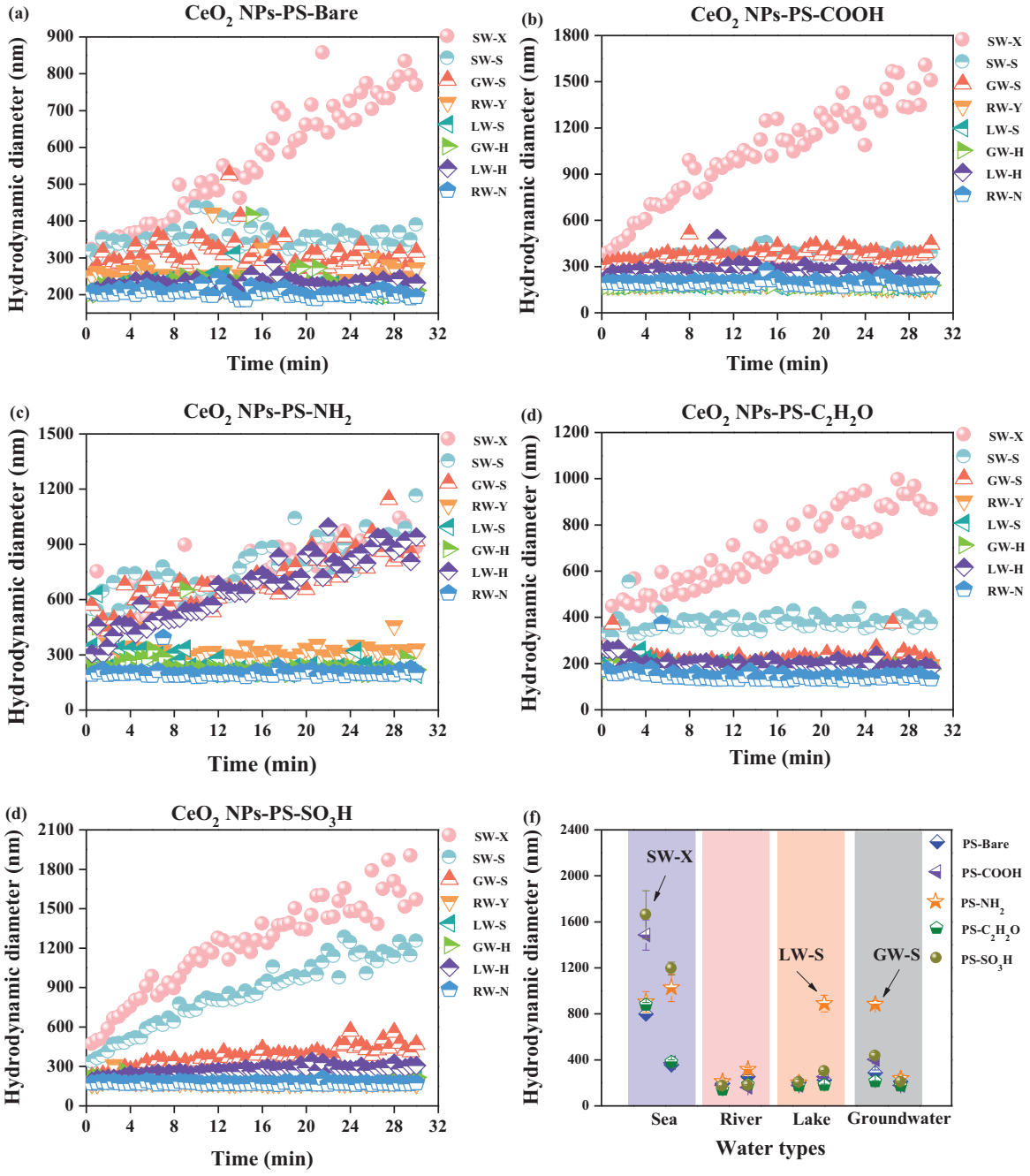

Fig. 1. Heteroaggregation kinetics of polystyrene nanoplastics (PS NPs) with ceria nanoparticles (CeO_2 NPs) in different types of water (a-e), and average hydrodynamic diameter of particles after heteroaggregation for 30 min.

charged PS-NH_2 and CeO_2 NPs, and destabilized the particles due to electrostatic screening. Based on this, we hypothesized that the interaction between PS NPs and CeO_2 NPs was related to the surface properties of PS NPs, as well as the composition of the receiving environment, especially with regard to IS and to NOM concentration. Hence, we further examined the individual contributions of pH, IS, and NOM concentration on the aggregation of the PS NPs as influenced by CeO_2 NPs in experimental conditions.

3.3. Homoaggregation

The TR-DLS has been widely applied in determining heteroaggregation kinetics and colloidal stability of a wide range of nanoparticles (Wang et al., 2015; Li et al., 2020). However, when two different particles are mixed in a solution, the obtained data with regard to the averaged diameter are system specific, and thus cannot quantify the aggregation rate of different particles, respectively. To better understand the influence of CeO_2 NPs on the aggregation and stability of PS NPs, homoaggregation attachment efficiencies (α) of five studied PS NPs and CeO_2 NPs were calculated based on their homoaggregation kinetics. The homoaggregation profile and attachment efficiency (α) of particles as a function of electrolyte concentration (NaCl and $CaCl_2$) are plotted in Fig. S3 and Fig. 3. The critical coagulation concentration (CCC), the minimum electrolyte concentration at which nanoparticles undergo favorable aggregation, is presented in Table 1. Generally, the aggregation behavior of CeO_2 NPs, PS-Bare, PS-COOH, PS-C_2H_2O, and PS-SO_3H in the two electrolyte solutions was

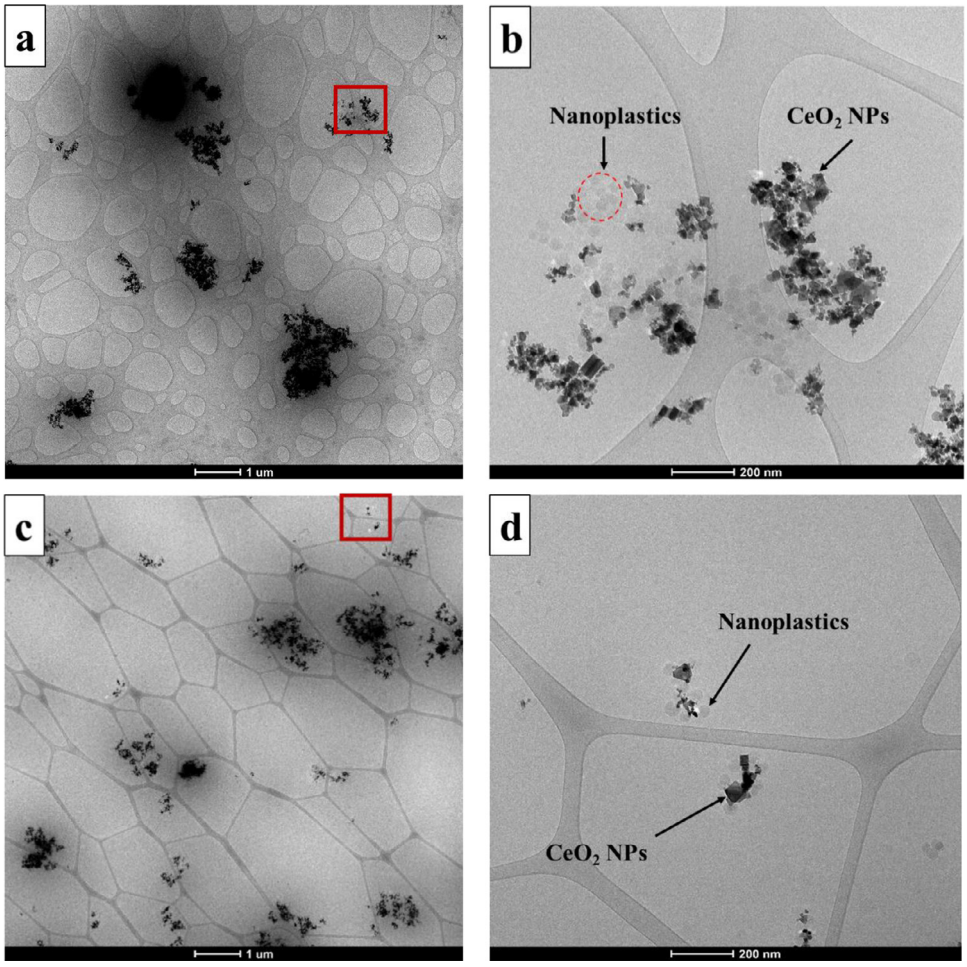

Fig. 2. Cryo-TEM images of polystyrene (PS) Bare nanoplastics and ceria nanoparrticles (CeO_2 NPs) in seawater (SW-X, a and b), and lake water (LW-H, c and d).

Table 1
The critical coagulation concentration (CCC) values of polystyrene nanoplastics (PS NPs) with different surface modifications in the presence and absence of ceria nanoparticles (CeO_2 NPs) at pH 5.0.

	CeO_2 NPs	PS-Bare	PS-COOH	PS-NH_2	PS-C_2H_2O	PS-SO_3H
NaCl	15.0	264	191	-	83.5	264
$CaCl_2$	10.0	29.1	16.0	-	10.1	29.0

	Binary system (CeO_2 NPs+)				
	PS-Bare	PS-COOH	PS-NH_2	PS-C_2H_2O	PS-SO_3H
NaCl	167	60.2	182	78.0	46.6
$CaCl_2$	20.4	7.50	27.0	10.8	1.70

consistent with the DLVO theory, suggesting that electrostatic interactions were the dominant stabilization mechanism (Yu et al., 2019; Fernando et al., 2020). The distinct reaction-limited regime (RLR) and the diffusion-limited regime (DLR) are illustrated in Fig. 3a and b. As the electrolyte concentration was lower than the CCC (in RLR), the D_h progressively increased with increasing electrolyte concentration because of charge screening or charge neutralization, as revealed by the increase of α (Fernando et al., 2020). As the electrolyte concentration exceeded the CCC (in DLR), the surface charge of particles was completely screened and the energy barrier between particles was eliminated, resulting in the aggregation rate reaching the maximum ($\alpha = 1$). Similar trends were also regularly observed for other ENPs (Yi et al., 2015; Fernando et al., 2020; Wang et al., 2019a). The CCCs for PS-Bare, PS-COOH, PS-C_2H_2O, and PS-SO_3H were 264, 191, 83.5, and 264 mM in NaCl, and 29.1, 16.0, 10.1, and 29.0 mM in $CaCl_2$, respectively. The observed CCCs of PS NPs were higher than for other ENPs, e.g. TiO_2 NPs (50 mM, NaCl) (Wang et al., 2015), CuO NPs (54.5 mM, NaCl) (Miao et al., 2016), and Ag NPs (12 mM, NaCl) (Fernando et al., 2020). This implies that the released PS NPs can well disperse in the surface water, and impair the organisms living in the water column due to chronic exposure (Zhang et al., 2019). The CCC_{Ca} of these four PS NPs was significantly lower than the CCC_{Na}, confirming that divalent electrolytes destabilized PS NPs suspensions more effectively than a monovalent electrolyte mainly because of their stronger charge neutralization ability (Singh et al., 2019), which

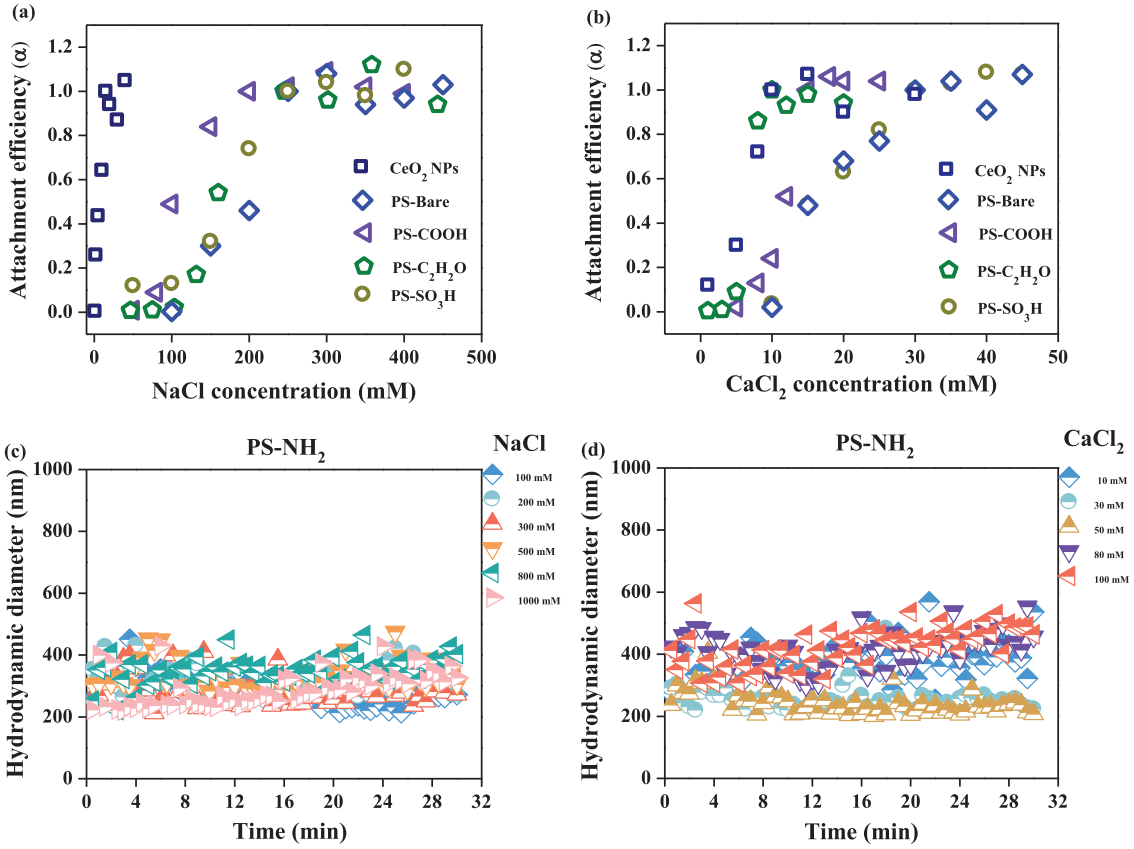

Fig. 3. Attachment efficiency of ceria nanoparticles (CeO_2 NPs) and polystyrene nanoplastics (PS NPs) with different surface modifications (a and b) as a function of NaCl and $CaCl_2$ concentrations at pH 5.0. Aggregation kinetics of PS-NH_2 at various NaCl (c) and $CaCl_2$ (d) concentrations at pH 5.0.

was also reported for other ENPs (Yi et al., 2015; Miao et al., 2016). The CCC ratio of $CaCl_2$ and NaCl was $2^{-3.18}$ for PS-Bare, $2^{-3.64}$ for PS-COOH, $2^{-3.05}$ for PS-C_2H_2O, and $2^{-3.18}$ for PS-SO_3H, which was in accordance with the Schulze–Hardy rule (the CCC ratio of $CaCl_2$ and NaCl should be in the range of z^{-6} to z^{-2}, where z is the valence of Ca^{2+}) (Chen and Huang, 2017).

Comparison of the CCCs of PS NPs with different functional groups revealed an obvious difference in their colloidal stability, which followed the sequence PS-C_2H_2O < PS-COOH < PS-SO_3H = PS-Bare ≪ PS-NH_2 at pH = 5 (Fig. 3 and Table 1). The lower salt tolerance of PS-C_2H_2O and PS-COOH seems related to the combined effects of double layer compression and cation complexation (Song et al., 2019). For positively charged PS-NH_2, the presence of electrolytes, even 1000 mM NaCl or 100 mM $CaCl_2$, had no or just a minor effect on its hydrodynamic size, suggesting that other non-DLVO interactions are involved in the stabilizing role (Fig. 3c and 3d). PS-NH_2 would remain stable in seawater or in electrolyte solutions, as already reported in previous studies (Dong et al., 2019; Yu et al., 2019). The high stability of PS-NH_2 may be derived from the branched polymer PEI chain layer on the surface of the PS NPs, which provides steric repulsion to overcome the electrostatic attraction (Yu et al., 2019; Ying et al., 2019). Overall, the difference in CCC values shows that surface functional groups have significant influences on the colloidal stability of PS NPs (Gewert et al., 2015; Yu et al., 2019).

3.4. Role of ionic strength and cation type

To explain the effects of positively charged CeO_2 NPs on the aggregation behavior of modified PS NPs, batch experiments of five PS NPs with different surface functional groups (PS-Bare, PS-COOH, PS-C_2H_2O, PS-NH_2, and PS-SO_3H) in the presence of CeO_2 NPs were performed in NaCl and $CaCl_2$ solutions at pH 5. As the concentration of electrolytes increased, the absolute values of the zeta potential progressively decreased, subsequently inducing an increase of the hydrodynamic diameter and the attachment efficiency (Fig. S4 and Fig. 4). Based on the comparison of the CCCs of PS NPs in the absence and presence of CeO_2 NPs, it clearly showed that the addition of CeO_2 NPs in both electrolyte solutions resulted in lower CCC values of the three negatively charged PS NPs (PS-Bare, PS-COOH, and PS-SO_3H), demonstrating the presence of metal-based nanoparticles aggravated the aggregation and sedimentation of PS NPs (Fig. 4, and Table 1). At pH 5, CeO_2 NPs, PS-Bare, PS-COOH, and PS-SO_3H were oppositely charged and well dispersed in the suspensions. When the anisotropic surface charges of the particles came together, the negatively charged PS NPs attached to positively charged CeO_2 NPs through electrostatic attraction (Yi et al., 2015; Li et al., 2020). This can be confirmed by the measured zeta potentials and calculated net energy barrier of the CeO_2 NPs – PS NPs heteroaggregates (Figs. 4c and d, and Fig. S5). However, although the hetero-system of PS-C_2H_2O and CeO_2 NPs followed the DLVO theory (Fig. S5g and S5h), negligible differences in the CCCs of PS-C_2H_2O were observed in the presence and absence of CeO_2 NPs (Table 1). This unexpected result can be caused by the epoxy group being capable of offering sorption sites for cations (Song et al., 2019). Hence, homoaggregates of PS-C_2H_2O were formed quickly even in the presence of CeO_2 NPs. Interestingly, the stability of positively charged PS-NH_2 in the copresence of CeO_2 NPs in NaCl and $CaCl_2$ suspensions was obviously different from that of single PS-NH_2 as shown in Figs. 3c and d, 4a and b. In salt solutions, the addition of CeO_2 NPs

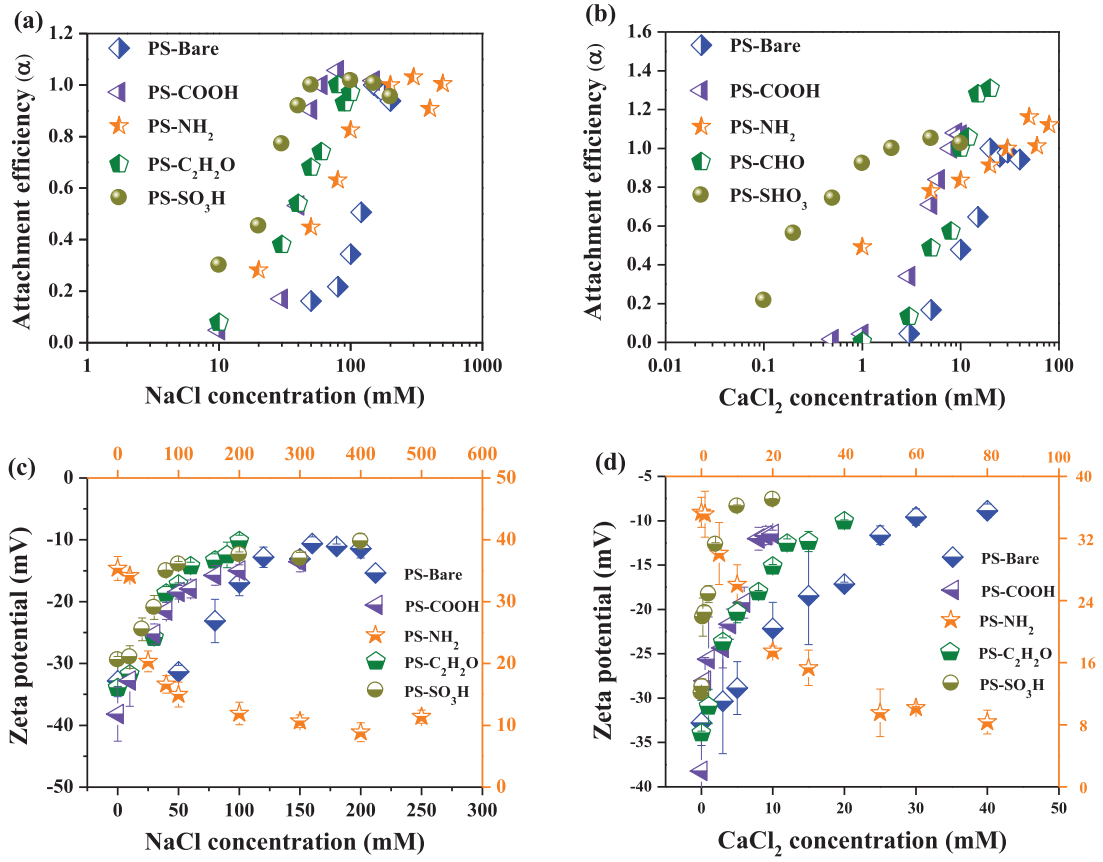

Fig. 4. Attachment efficiency (a and b) and corresponding zeta potential (c and d) of polystyrene nanoplastics (PS NPs) in the presence of ceria nanoparticles (CeO_2 NPs) and as a function of NaCl and $CaCl_2$ concentrations at pH 5.0.

induced significant aggregation of PS-NH_2 (e.g. CCC_{Na} = 181.6 mM, CCC_{Ca} = 27 mM), while single PS-NH_2 remained stable even in 1000 mM NaCl and 100 mM $CaCl_2$ (Fig. 4 and Table 1). According to DLVO theory, electrostatic repulsion dominates the behavior of two isotropic charged particles, e.g. carbon nanocapsules – montmorillonite (Lan and Cheng, 2012), graphene oxide – goethite (Zhao et al., 2015), and biochar NPs – kaolin (Liu et al., 2018). The contradictory result obtained in this study indicates that other non-electrostatic interactions played an important role in the adsorption of PS-NH_2 to CeO_2 NPs, as discussed below.

Generally, classical DLVO theory is widely applied to elaborate the interactions between particles (Wang et al., 2015; Li et al., 2020). However, other non-DLVO interactions, e.g. hydrogen force, chemical bonding, π-π interaction or steric repulsion, also participate in the attachment process of carbon materials (Lu et al., 2018; Song et al., 2019; Tan et al., 2019). The surface composition of PS NPs heteroaggrergated with CeO_2 NPs under simulated natural environmental was determined to understand the underlying interaction mechanisms. As shown in Fig. S6a, XPS C1s spectra of PS-Bare displayed that the peak at 291.33 eV decreased slightly after heteroaggregation with CeO_2 NPs, meaning that π-π interaction force contributed to the heteroaggregation of PS NPs and CeO_2 NPs (Fig. 5a) (Lu et al., 2018). To further identify the role of surface functional groups, the chemical functional groups of PS NPs, before and after interaction with CeO_2 NPs and electrolytes were analyzed by FTIR (Figs. 5b–f). The peak at 756 cm^{-1} is assigned to an aromatic group, which can bind strongly with cations because of the presence of π-electrons (Harvey et al., 2011). The decrease of intensity of the peak of the aromatic group after heteroaggregation suggests the involvement of the aromatic group in the heteroaggregation of CeO_2 NPs and PS NPs. The bands at 1601, and 3419~3434 cm^{-1} correspond to C=C and -OH, respectively (Wang et al., 2019a). They increased in intensity after heteroaggregation. This is in agreement with the observations of Lu et al. (2018), indicating the presence of hydrated cations adsorbed on the surface of PS NPs. Compared to PS-Bare, the new bands of 1324 cm^{-1} in PS-COOH (Liu et al., 2013), 698 cm^{-1} and 3450 cm^{-1} in PS-NH_2 (Feng et al., 2019), 908 and 1181 cm^{-1} in PS-C_2H_2O (Ho et al., 2017; Yang et al., 2019a), and 620 cm^{-1} in PS-SO_3H (Bosque et al., 2014), are the evidence of functional groups grafting on the surface of PS NPs. After heteroaggregation for 30 min, the intensity of these peaks decreased, confirming that functional groups contributed to CeO_2 NPs and electrolytes adsorption to PS NPs. Hence, PS-COOH, PS-C_2H_2O, and PS-SO_3H, were more prone to attachment to CeO_2 NPs in the presence of electrolytes, as compared to PS-Bare. These results also indicated us that plastics debris may increasingly tend to heteroaggregate with ENPs as plastics are ageing, which thus increases exposure risk to benthic organisms.

3.5. Role of solution pH

The pH-dependent charge changes are commonly reported for ENPs and correlated with their colloidal stability and aggregation behavior (Wang et al., 2019b). Exposing CeO_2 NPs and PS-NPs to various pH levels (pH = 5, 7, and 9), caused significant differences in diameter increase and colloidal stability, as shown in Fig. S7 and Fig. 6. The attachment efficiencies of PS NPs in the presence of CeO_2 NPs displayed similar trends under two electrolytes. At pH 5, fast aggregation was observed, and the corresponding α was fixed at 1. Upon pH increase, the α obtained from negatively charged PS NPs decreased significantly, indicating that high pH inhibited the

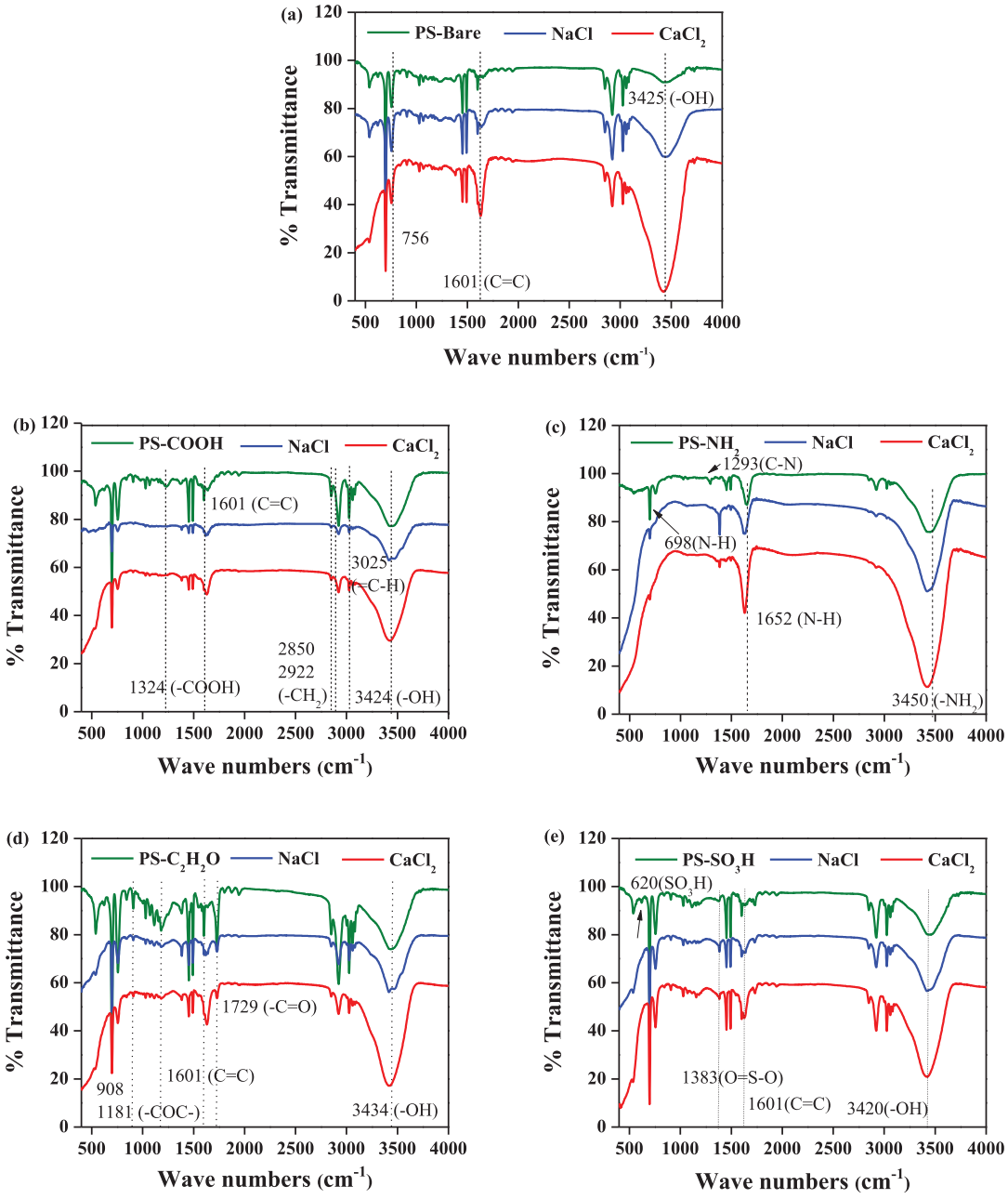

Fig. 5. FTIR spectra of polystyrene nanoplastics (PS NPs) in the co-presence of ceria nanoparticles (CeO_2 NPs) and NaCl, or $CaCl_2$ solution, respectively (a-e).

heteroaggregation between negatively charged PS NPs and CeO_2 NPs. Wang et al. (2019b) also observed that the heteroaggregates of n-ZVI and clay mineral particles were smaller at pH 9.5 than at pH 6.5. The particles possessed a more negative surface charge as pH increased to 9, which further increased electrostatic repulsion and the energy barrier among particles, and in turn stabilized the particles (Mao et al., 2020). In contrast, an increased pH led to a higher value of α for positively charged PS-NH_2 (except for NaCl at pH 9). At pH = 7, being the pH at which the surface charges of PS-NH_2 and CeO_2 NPs were close to zero with minimal electrostatic repulsion between the particles, fast heteroaggregation occurred (Fig. S2a and 2d). A similar phenomenon also has been reported by Yi et al. (2015), who found that heteroaggregation of nanoparticles of pyrolyzed biomass and CeO_2 NPs occurred at pH 7.1. They concluded that this heteroaggregation was induced by a core−shell stabilization mechanism. Hence, we speculates that core−shell stabilization may have contributed to the heteroaggregation of PS-NH_2 and CeO_2 NPs: PS-NH_2 can bind to and form a positively charged shell on the neutral surface of the nascent CeO_2 NPs core. As pH further increased from 7 to 9, the aggregation rate was reduced due to the increase in electrostatic repulsion, as confirmed by the corresponding zeta potential of the PS-NH_2 and CeO_2 NPs (Fig. S2a and 2d).

3.6. Role of humic acid

Humic acid is widely distributed in the natural aquatic environment and plays a critical role in driving the stability, dissolution, and transport of ENPs (Philippe et al., 2014; Li et al., 2020). In this study, the role of HA was clearly corroborated by the behavior of α as a function of the concentrations of HA at fixed electrolyte concentrations (Fig. S8 and Fig. 7). Overall, the effects of HA concentrations varied depending on the PS NPs functional groups and

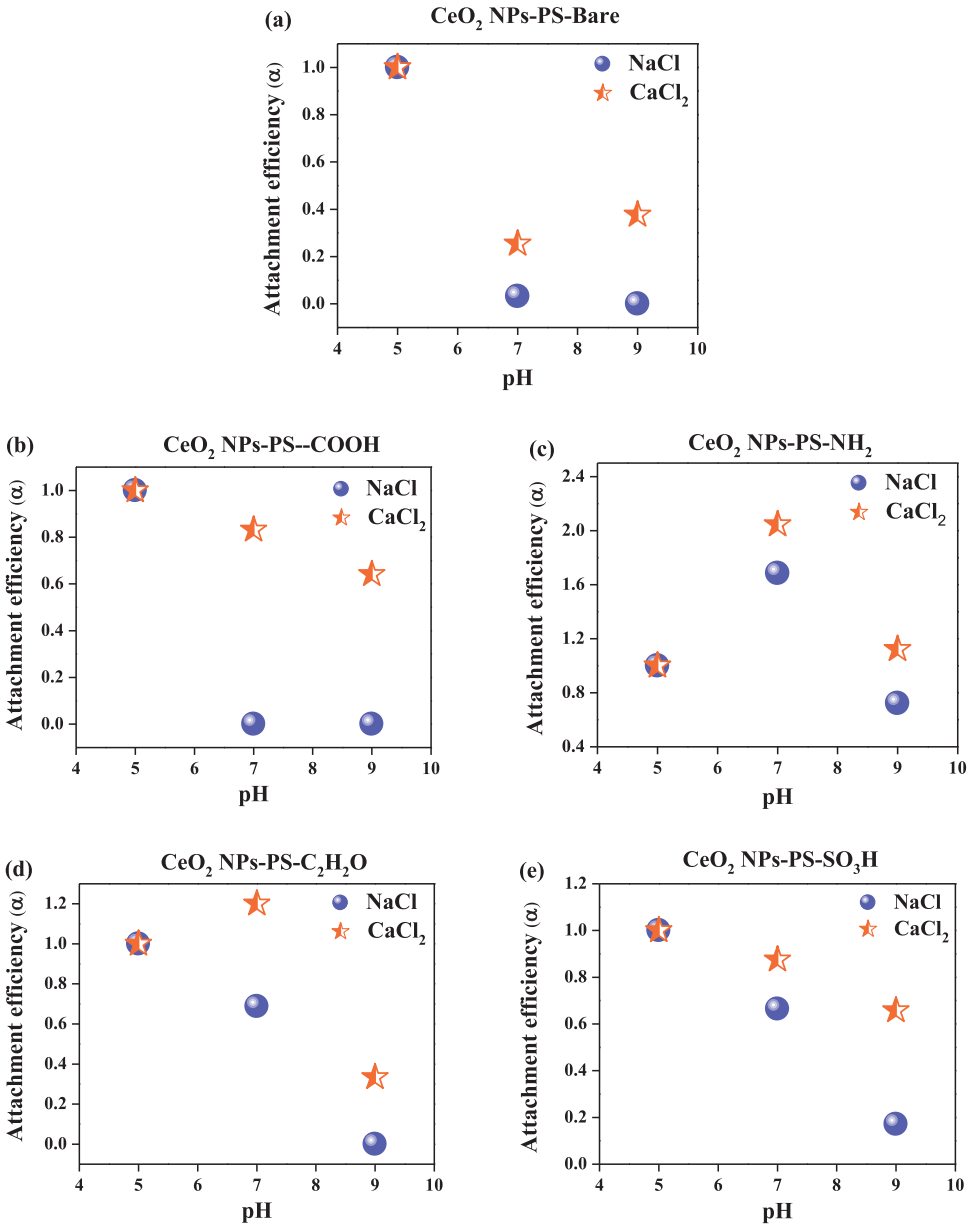

Fig. 6. Effect of pH on the fast aggregation of polystyrene nanoplastics (PS NPs) with different surface modifications with ceria nanoparticles (CeO_2 NPs) in NaCl and $CaCl_2$ solutions. The attachment efficiency was calculated by normalizing the aggregation rate at the critical coagulation concentration (CCC).

the cation type. For NaCl, a value of $\alpha > 1$ was observed for three PS NPs (PS-Bare, PS-COOH, and PS-NH_2) in the presence of 0.1 mg C/L HA. This can be attributed to charge neutralization (Wu et al., 2019), as confirmed by the decrease of the zeta potential (Figs. S7a, 7b and 7c). However, addition of 0.1 mg C/L HA enhanced the stability of PS-C_2H_2O and PS-SO_3H. This opposite result observed for the five PS NPs again indicates that their surface properties should be taken into consideration when assessing their colloidal stability. As the HA concentration further increased from 0.1 to 10 mg C/L, the value of α for the five PS NPs decreased gradually, accompanied with a decrease of the corresponding zeta potential (Fig. 5 and Fig. S9). This reduction can be interpreted by electrostatic and steric effects resulting from the adsorption of HA onto the surface of PS NPs and CeO_2 NPs, as reported for gold nanoparticles (Liu et al., 2013), black phosphorus (Tan et al., 2019), and biochar colloids (Yang et al., 2019b). The analysis of O1s spectra of PS-Bare displayed that the binding energy in the position of 532.15 eV (C=O) and 533.24 eV (C-O) decreased, further confirming HA was adsorbed on the surface of heteroaggregates (Fig. S6) (Wang et al., 2020). Unlike in NaCl solutions, significant heteroaggregation was observed in $CaCl_2$ solutions at any HA concentration studied. This suggests that divalent cations possess a higher efficiency in destabilizing NPs than monovalent cations (Yu et al., 2019; Li et al., 2020). When the concentration of HA was lower than 5 mg C/L, aggregation of both PS-Bare and PS-NH_2 was promoted by HA due to the cation bridging effect and double layer compression (Fig. 7) (Singh et al., 2019). In contrast, the stability of PS-COOH, PS-C_2H_2O and PS-SO_3H was increased. At low HA concentration (< 5 mg C/L), large amounts of HA molecules were adsorbed on the surface of the three particles, and a limited number of HA molecules can bind with Ca^{2+} to form larger clusters (Yu et al., 2019). Furthermore, the addition of 10 mg C/L HA effectively reduced the aggregation of the five PS NPs studied. This stabilizing effect may arise from steric repulsion because of the adsorption of HA onto the surface of the particles (Liu et al., 2013; Li et al., 2020). Compared to negatively charged PS NPs, the presence of 10 mg C/L HA had a limited effect

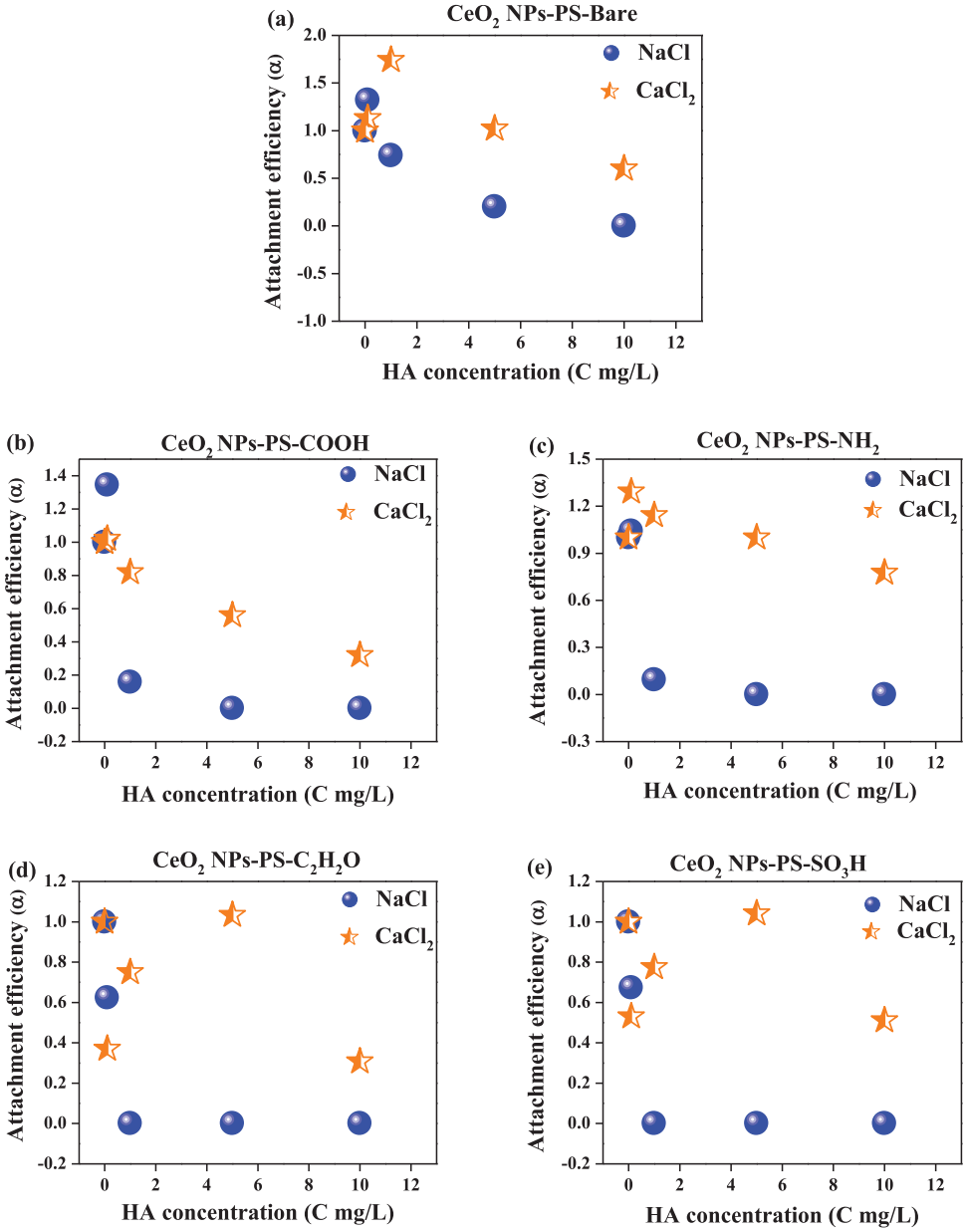

Fig. 7. Effect of HA concentration on the fast aggregation of polystyrene nanoplastics (PS NPs) with different surface modifications with ceria nanoparticles (CeO_2 NPs) in NaCl and $CaCl_2$ solutions at pH 5.0. The attachment efficiency was calculated by normalizing the aggregation rate at the critical coagulation concentration (CCC).

on the heteroaggregation of PS-NH_2 and CeO_2 NPs (Fig. 7 and Fig. S8). This can be explained by the fact that the steric repulsion is weaker than the Ca^{2+} bridging effect (Yang et al., 2019b).

4. Conclusions

Interactions between PS NPs and non-plastic CeO_2 NPs may occur because CeO_2 NPs particles are prevalently present in aquatic environments. This study is the first to investigate the aggregation behavior of PS NPs with different surface modification, as influenced by CeO_2 NPs as well as environmental factors (pH, ionic strength, cation type and humic acid). Results revealed that CeO_2 NPs could form heteroaggregates with both negatively and positively charged PS NPs in high ionic compositions (e.g. SW-X) due to charge screening. In GW-S, limited aggregation was found for the four negatively charged PS NPs, but obvious aggregation happened in PS-NH_2 – CeO_2 NPs suspensions. These different processes can mainly be ascribed to the surface charge of the particles and the high content of anions in GW-S. The presence of CeO_2 NPs effectively destabilized four PS NPs, including PS-Bare, PS-COOH, PS-NH_2, and PS-SO_3H, in both NaCl and $CaCl_2$ solutions because of electrostatic neutralization and adsorption of functional groups. It is concluded that a neutral environment facilitates the heteroaggregation of PS-NH_2 and CeO_2 NPs, whilst enhancing the stability of negatively charged PS NPs and CeO_2 NPs. The heteroaggregation kinetics of PS NPs and CeO_2 NPs was also influenced by the surface functional groups of PS NPs, HA concentrations, and the interaction of functional groups, HA and cations. These results highlight the importance of surface coating of PS NPs in understanding the aggregation, transport, and the eventual fate of PS NPs, and provide profound insight into their actual environmental behavior.

Declaration of Competing Interest

There is no competing interest to declare.

Acknowledgements

This study was supported by the National Natural Science Foundation of China (No. 41877500, No. 41701571, No. 41701573, and No. 41977115), Shanghai Rising-Star Program (No. 20QA1404500), the National Key R&D Program of China (No. 2018YFC1800600, No. 2018YFD0800700), Science and Technology Program of Guangzhou, China (No. 201904010116).

Supplementary materials

Supplementary material associated with this article can be found, in the online version, at doi:10.1016/j.watres.2020.116324.

References

Blettler, M.C.M., Garello, N., Ginon, L., Abrial, E., Wantzen, K.M., 2019. Massive plastic pollution in a mega-river of a developing country: sediment deposition and ingestion by fish (*Prochilodus lineatus*). Environ. Pollut. 255, 113348.

Bosque, I.F.S.D., Ramírez, M., Blanco-Varela, M.T., 2014. FTIR study of the effect of temperature and nanosilica on the nanostructure of C-S-H gel formed by hydrating tricalcium silicate. Constr. Build. Mater. 52, 314–323.

Cai, L., He, L., Peng, S.N., Li, M., Tong, M.P., 2019. Influence of titanium dioxide nanoparticles on the transport and deposition of microplastics in quartz sand. Environ. Pollut. 253, 351–357.

Cai, L., Hu, L., Shi, H., Ye, J., Zhang, Y., Kim, H., 2018. Effects of inorganic ions and natural organic matter on the aggregation of nanoplastics. Chemosphere 197, 142–151.

Chen, C.Y., Huang, W.L., 2017. Aggregation kinetics of nanosized activated carbons in aquatic environments. Chem. Eng. J. 313, 882–889.

Chen, K.L., Elimelech, M, 2006. Aggregation and deposition kinetics of fullerene (C_{60}) nanoparticles. Langmuir 22, 10994–11001.

Cole, M., Galloway, T.S., 2015. Ingestion of nanoplastics and microplastics by *Pacific oyster larvae*. Environ. Sci. Technol. 49, 14625–14632.

Cózar, A., Echevarria, F., Gonzalez-Gordillo, J.I., Irigoien, X., Ubeda, B., Len, S.H., 2014. From the cover: plastic debris in the open ocean. Proc. Natl. Acad. Sci. 111, 10239.

Dawson, A.L., Kawaguchi, S., King, C.K., Townsend, K.A., King, R., Huston, W.M., Nash, S.M.B., 2018. Turning microplastics into nanoplastics through digestive fragmentation by *Antarctic krill*. Nat. Commun. 9, 1001.

Dong, Z.Q., Zhang, W., Qiu, Y.P., Yang, Z.L., Wang, J.L., Zhang, Y.D., 2019. Cotransport of nanoplastics (NPs) with fullerene (C_{60}) in saturated sand: Effect of NPs/C_{60} ratio and seawater salinity. Water Res. 148 (1), 468–478.

Enfrin, M., Duméed, L.F., Lee, J., 2019. Nano/microplastics in water and wastewater treatment processes – origin, impact and potential solutions. Water Res. 161 (15), 621–638.

Enfrin, M., Lee, J., Gibert, Y., Basheer, F., Kong, L.X., Duméed, L.F., 2020. Release of hazardous nanoplastic contaminants due to microplastics fragmentation under shear stress forces. J. Hazar. Mater. 384 (15), 121393.

Enfrin, M., Lee, J., Le-Clech, P., Duméed, L.F., 2020. Kinetic and mechanistic aspects of ultrafiltration membrane fouling by nano- and microplastics. J. Membr. Sci. 601 (1), 117890.

Fall, M., Guerbet, M., Park, B., Gouriou, F., Dionnet, F., Morin, J.P., 2007. Evaluation of cerium oxide and cerium oxide based fuel additive safety on organotypic cultures of lungslices. Nanotoxicology 1 (3), 227–234.

Feng, L.J., Li, J.W., Xu, E.G., Sun, X.D., Yuan, X.Z., 2019. Short-term exposure of positively charged polystyrene nanoparticles causes oxidative stress and membrane destruction in cyanobacteria. Environ. Sci.: Nano 6, 3072–3079.

Fernando, I., Lu, D., Zhou, Y., 2020. Interactive influence of extracellular polymeric substances (EPS) and electrolytes on the colloidal stability of silver nanoparticles. Environ. Sci.: Nano 7, 186–197.

Gewert, B., Plassmann, M.M., MacLeod, M., 2015. Pathways for degradation of plastic polymers floating in the marine environment. Environ. Sci.: Proc. Imp. 17 (9), 1513–1521.

Halle, A.T., Ladirat, L., Gendre, X., Goudoun, D., Pusineri, C., Routaboul, C., Tenailleau, C., Duployer, B., Perez, E., 2016. Understanding the fragmentation pattern of marine plastic debris. Environ. Sci. Technol. 50, 5668–5675.

Harvey, O.R., Herbert, B.E., Rhue, R.D., Kuo, L.J., 2011. Metal interactions at the biochar-water interface: energetics and structure-sorption relationships elucidated by flow adsorption microcalorimetry. Environ. Sci. Technol. 45, 5550–5556.

He, B.B., Goonetilleke, A., Ayoko, G.A., Rintoul, L., 2020. Abundance, distribution patterns, and identification of microplastics in Brisbane river sediments, Australia. Sci. Total Environ. 700, 134467.

Hernandez, L.M., Yousefi, N., Tufenkji, N., 2017. Are there nanoplastics in your personal care products? Environ. Sci. Technol. Lett. 4, 280–285.

Ho, S.H., Chen, Y.D., Yang, Z.K.Nagarajan, D., Chang, J.S., Ren N.Q., 2017. High-efficiency removal of lead from wastewater by biochar derived from anaerobic digestion sludge. Bioresour. Technol 246, 142–149.

Lan, Y.F., Cheng, S.C., 2012. Dispersion of carbon nanocapsules by using highly aspect-ratio clays. Appl. Phys. Lett. 100, 153109.

Li, S.C., Liu, H., Gao, R., Abdurahman, A., Dai, J., Zeng, F., 2018. Aggregation kinetics of microplastics in aquatic environment: complex roles of electrolytes, pH, and natural organic matter. Environ. Pollut. 237, 126–132.

Li, X., He, E.K., Zhang, M.Y., Peijnenburg, W.J.G.M., Liu, Y., Song, L., Cao, X.D., Zhao, L., Qiu, H., 2020. Interactions of CeO_2 nanoparticles with natural colloids and electrolytes impact their aggregation kinetics and colloidal stability. J. Hazard Mater. 386 (15), 121973.

Liu, G.C., Zheng, H., Jiang, Z.X., Wang, Z.Y., 2018. Effects of biochar input on the properties of soil nanoparticles and dispersion/sedimentation of natural mineral nanoparticles in aqueous phase. Sci. Total Environ. 634, 595–605.

Liu, J.F., Legros, S., Kammer, F.V.D., Hofmann, T., 2013. Natural organic matter concentration and hydrochemistry influence aggregation kinetics of functionalized engineered nanoparticles. Environ. Sci. Technol. 47, 4113–4120.

Lodeiro, P., Achterberg, E.P., Rey-Castro, C., El-Shahawi, M.S., 2018. Effect of polymer coating composition on the aggregation rates of Ag nanoparticles in NaCl solutions and seawaters. Sci. Total Environ. 631-632, 1153–1162.

Lorenz, C., Roscher, L., Meyer, M.S., Hildebrandt, L., Prume, J., Loder, M.G.J., Primpke, S., Gerdts, G., 2019. Spatial distribution of microplastics in sediments and surface waters of the southern North Sea. Environ. Pollut. 252, 1719–1729.

Lu, S.H., Zhu, K.L., Song, W.C., Song, G., Chen, D.Y., Hayat, T., Alharbi, N.S., Chen, C.L., Sun, Y.B., 2018. Impact of water chemistry on surface charge and aggregation of polystyrene microspheres suspensions. Sci. Total Environ. 630, 951–959.

Mao, Y.F., Li, H., Huangfu, X.L., Liu, Y., He, Q., 2020. Nanoplastics display strong stability in aqueous environments: insights from aggregation behaviour and theoretical calculations. Environ. Pollut. 258, 113760.

Miao, L.Z., Wang, C., Hou, J., Wang, P.F., Ao, Y.H., Li, Y., Lv, B.W., You, G.X., Xu, Y., 2016. Effect of alginate on the aggregation kinetics of copper oxide nanoparticles (CuO NPs): bridging interaction and hetero-aggregation induced by Ca^{2+}. Environ. Sci. Pollut. R. 23, 11611–11619.

Napper, I.E., Thompson, R.C., 2016. Release of synthetic microplastic plastic fibres from domestic washing machines: effects of fabric type and washing conditions. Mar. Pollut. Bull. 112, 39–45.

Oriekhova, O., Stoll, S., 2018. Heteroaggregation of nanoplastic particles in the presence of inorganic colloids and natural organic matter. Environ. Sci.: Nano 5, 792–799.

Philippe, A., Schaumann, G.E., 2014. Interactions of dissolved organic matter with natural and engineered inorganic colloids: a review. Environ. Sci. Technol. 48 (16), 8946–8962.

Piccinno, F., Gottschalk, F., Seeger, S., Nowack, B., 2012. Industrial production quantities and uses of ten engineered nanomaterials in Europe and the world. J. Nanopart. Res. 14, 1–11.

Singh, N., Tiwari, E., Khandelwal, N., Darbha, G.K., 2019. Understanding the stability of nanoplastics in aqueous environments: effect of ionic strength, temperature, dissolved organic matter, clay, and heavy metals. Environ. Sci.: Nano 6, 2968–2976.

Song, B.Q., Chen, M., Zhao, L., Qiu, H., Cao, X.D., 2019. Physicochemical property and colloidal stability of micron- and nano- particle biochar derived from a variety of feedstock sources. Sci. Total Environ. 661 (15), 685–695.

Tan, Z.Q., Yin, Y.G., Guo, X.R., Wang, B.W., Shang, H.P., Xu, J.W., Zhao, Q., Liu, J.F., Xin, B.S., 2019. Natural organic matter inhibits aggregation of few-layered black phosphorus in mono- and divalent electrolyte solutions. Environ. Sci.: Nano 6, 599–609.

Tiwari, E., Mondal, M., Singh, N., Khandelwal, N., Monikh, F.A., Darbha, G.K., 2020. Effect of the irrigation water type and other environmental parameters on CeO_2 nanopesticide–clay colloid interactions. Environ. Sci.: Proc. Imp. 22, 84–94.

Wang, H.T., Dong, Y.N., Zhu, M., Li, X., Keller, A.A., Wang, T., Li, F.T., 2015. Heteroaggregation of engineered nanoparticles and kaolin clays in aqueous environments. Water Res. 80, 130–138.

Wang, J.Y., Zhao, X.L, Wu, A.M., Tang, Z., Niu, L., Wu, F., Wang, F.C., Zhao, T.H., Fu, Z.Y., 2020. Aggregation and stability of sulfate-modified polystyrene nanoplastics in synthetic and natural waters. Environ. Pollut., 114240.

Wang, X.D., Li, C.X., Li, Z.W., Yu, G.W., Wang, Y., 2019. Effect of pyrolysis temperature on characteristics, chemical speciation and risk evaluation of heavy metals in biochar derived from textile dyeing sludge. Ecotox. Environ. Safe. 168, 45–52.

Wang, Y.L., Yang, K., Chefetz, B., Xing, B.S., Lin, D.H., 2019. The pH and concentration dependent interfacial interaction and heteroaggregation between nanoparticulate zero-valent iron and clay mineral particles. Environ. Sci.: Nano 6, 2129.

Wright, S.L., Thompson, R.C., Galloway, T.S., 2013. The physical impacts of microplastics on marine organisms: a review. Environ. Pollut. 178, 483–492.

Wu, J.Y., Jiang, R.F., Lin, W., Ouyang, G.F., 2019. Effect of salinity and humic acid on the aggregation and toxicity of polystyrene nanoplastics with different functional groups and charges. Environ. Pollut. 245, 835–843.

Yang, D.X., Li, L.F., Chen, B.L., Shi, S.X., Nie, J., Ma, G.P., 2019. Functionalized chitosan electrospun nanofiber membranes for heavy-metal removal. Polymer 163, 74–85.

Yang, W., Shang, J.Y., Sharma, P., Li, B.G., Liu, K.S., Flury, M., 2019. Colloidal stability and aggregation kinetics of biochar colloids: effects of pyrolysis temperature, cation type, and humic acid concentrations. Sci. Total Environ. 658, 1306–1315.

Yi, P., Pignatello, J.J., Uchimiya, M., White, J.C., 2015. Heteroaggregation of cerium oxide nanoparticles and nanoparticles of pyrolyzed biomass. Environ. Sci. Technol. 49, 13294–13303.

Ying, Y.H., Wang, Z.X., Wan, S.J., Pu, J.W., 2019. Cellulose-based formaldehyde adsorbents with large capacities: efficient use of polyethylenimine for graphene oxide stabilization in alkaline-urea system. J. Appl. Polym. Sci. 136 (34), 47860.

Yu, S.J., Shen, M.H., Li, S.S., Fu, Y.J., Zhang, D., Liu, H.Y., Liu, J.F., 2019. Aggregation kinetics of different surface-modified polystyrene nanoparticles in monovalent and divalent electrolytes. Environ. Pollut. 255, 113302.

Zhang, F., Wang, Z., Wang, S., Fang, H., Wang, D.G., 2019. Aquatic behavior and toxicity of polystyrene nanoplastic particles with different functional groups: complex roles of pH, dissolved organic carbon and divalent cations. Chemosphere 228, 195–203.

Zhang, K., Xiong, X., Hu, H.J., Wu, C.X., Bi, Y.H., Wu, Y.H., Zhou, B.S., Lam, P.K.S., Liu, J.T., 2017. Occurrence and characteristics of microplastic pollution in Xiangxi Bay of three gorges reservoir. China, Environ. Sci. Technol. 51, 3794–3801.

Zhao, J., Dai, Y.H., Wang, Z.Y., Ren, W.T., Wei, Y.P., Cao, X.S., Xing, B.S., 2018. Toxicity of GO to freshwater algae in the presence of Al_2O_3 particles with different morphologies: importance of heteroaggregation. Environ. Sci. Technol. 52, 13448–13456.

Zhao, J., Liu, F., Wang, Z., Cao, X.S., Xing, B.S., 2015. Heteroaggregation of graphene oxide with minerals in aqueous phase. Environ. Sci. Technol. 49, 2849–2857.